Smart Structures and Systems, *Vol. 35*, *No. 5* (*2025*) *235-252*
https://doi.org/10.12989/sss.2025.35.5.235

Performance enhancement of an intelligent isolation system based on deep deterministic policy gradient

Tzu-Kang Lin [1a], Chandrasekhara Tappiti [2b], Lyan-Ywan Lu*[2] and Ko Yi Chen [1c]

[1] *Department of Civil Engineering*, *National Yang Ming Chiao Tung University*, *Hsinchu city*, *Taiwan*
[2] *Department of Civil Engineering*, *National Cheng Kung University*, *Tainan*, *Taiwan*

(*Received November 19*, *2024*, *Revised May 16*, *2025*, *Accepted June 2*, *2025*)

Abstract. Regions within the seismic zone of the pacific volcanic quadrant are highly susceptible to frequent seismic activity, posing significant threats to both human life and infrastructure. This threat is particularly critical for the high-tech industries, which are holding a substantial global market share and highly vulnerable to earthquake-induced damages. The characteristics of earthquake ground motion play a crucial role in the effectiveness of structural control systems, especially for near-fault earthquakes, where low-frequency resonance can cause significant displacement in the isolation layer. To address these challenges, this study focuses on advancement of smart structural systems through the development of an intelligent semi-active isolation system using an innovative control strategy based on artificial intelligence. Specially, the study employs the deep deterministic policy gradient (DDPG) algorithm to enhance the control of seismic isolations systems. The control modules are tailored for distinct characteristics of both near-fault and far-field seismic events, ensuring effective mitigation of seismic impacts. The results demonstrate significant enhancements in structural performance using the DDPG-based framework, showing a reduction of approximately 68.85% in isolation layer displacement during near-fault earthquakes and a 57.65% reduction in superstructure acceleration during far-field earthquakes. These outcomes affirm the effectiveness of the DDPG-driven intelligent control strategies for advancing the resilience and service life of critical infrastructures in seismically active regions, contributing to the broader fields of structural control and prognosis.

Keywords: artificial intelligent; deep deterministic policy gradient algorithm; ground motion characteristics; seismic isolation; seismic resilience; semi-active control; smart structures

1. Introduction

Regions located along the continental plate boundaries of the Pacific rim are vulnerable to frequent seismic events. These earthquakes pose significant risks, particularly due to high population density and diverse geological conditions, which affect urban high-rises and industries such as semiconductors. The statistics indicate that thousands of earthquakes occur annually, with some resulting in substantial economic losses, especially impacting vital high-tech sectors like cloud computing. Over 800 seismic stations have played a crucial role in enhancing the understanding and implementation of structural control technologies in these areas. These includes passive, active, and semi-active controls, which are crucial for minimizing damage to buildings and sensitive manufacturing equipment. The focus of recent studies has been on developing semi-active control techniques that are specifically tailored to unique seismic characteristics. Therefore, the aim of the proposed investigation is to optimize structural response and reduce damage during earthquakes, which is crucial for protecting life, property, and the high-tech export industry.

Despite advances in science and technology, precise earthquake predictions remain elusive, emphasising the importance of continuous improvement in early warning systems and public awareness through emergency drills and education. It was found by numerous authors that a pulse-like shape in the surface motion velocity history could be observed at observation stations near faults. It was hypothesised that this phenomenon was caused by the rupture directivity effect, which resulted from the S waves of earthquakes travelling along the faults. Furthermore, it was suggested that the seismic S-waves along the fault rupture direction gradually superimposed, leading to an accumulation of energy (Baker 2007, Shahi and Baker 2011, Spudich *et al*. 2014). Similarly, near-fault earthquakes exhibit larger peak velocities and displacements, with energy typically concentrated in one or multiple pulses (Pavlidou and Komodromos 2020, Moustafa and Takewaki 2010).

Structural control is categorised into passive, active, and semi-active control, with the latter combining the benefits of both. Dynamic response is inhibited through vibration isolation and energy dissipation. The Friction Damper Device (FDD), developed by Imad *et al*. effectively reduces inter-story displacement and shear when properly

*Corresponding author, Ph.D., Professor,
E-mail: lylu@ncku.edu.tw
[a] Professor
[b] Postdoctoral fellow
[c] Research assistant

ISSN: 1738-1584 (Print), 1738-1991 (Online)

configured (Mualla and Belev 2002). Numerous studies have explored on optimizing structural resilience and control in steel plate connections and steel structures, highlighting on sustainability and seismic protection through advanced modelling and energy redistribution strategies. These approaches, including intermodal targeted energy transfer, effectively redistribute seismic energy between structural modes, enhancing seismic performance of tall buildings and offering a promising solution for seismic protection in high-rise buildings (Gzal *et al*. 2023, Shi *et al*. 2024). Self-centering seismic base isolators, which incorporate super elastic shape memory alloys (SMAs), are used to enhance structural resilience and attenuate residual displacements after earthquakes. SMAs, known for their energy dissipation efficiency, fatigue resistance, and durability under large strain, can be customized by adjusting the number of SMA cores to meet various seismic control requirements (Dolce *et al*. 2000, Eswar *et al*. 2022, Wang *et al*. 2020).

The semi-active control concept involves detecting and feeding back the structural system's dynamic response via sensors and adjusting control parameters accordingly. Unlike hybrid and active control systems, requires less energy and offers superior suppression of dynamic responses through real-time adjustments (Yang and Agrawal 2002). Furthermore, the Negative Stiffness Inerter System (NSIS) is designed to enhance earthquake protection in structural systems by combining a negative stiffness mechanism with an inerter to reduce seismic responses. The system improves energy dissipation and stability during earthquake excitations, showing superior isolation performance compared to traditional passive control methods, particularly under strong seismic forces (Zhao *et al*. 2020). The computational modelling of piezoelectric actuators output performance under voltage excitation poses challenges in determining actuator voltages during dynamic excitations. Nevertheless, the precision findings enhance the precision and control in applications involving piezoelectric actuators in smart materials and adaptive structures (Fang *et al*. 2024). Liu *et al*. introduced a half-active variable damping and stiffness system, consists of two MR dampers and two linear springs. Numerical simulations and experimental validation demonstrated excellent vibration isolation by adjusting damping and stiffness for various shock waves (Liu *et al*. 2008). A six-directional vibrating table was used to conduct the fuzzy control experiments, using the Short-Term Average/Long-Term Average method to determine the occurrence and triggering point of earthquake events. This was achieved by analysing vertically and horizontally oriented historical data through on-site monitoring (Lin *et al*. 2023, Kim *et al*. 2006). However, a hybrid control strategy for smart base-isolated buildings that combines model-based and data-driven approaches to address uncertainties in system behavior are also developed. It demonstrates, through simulations, the effectiveness of these strategies in enhancing the performance of buildings under seismic loading by integrating prior knowledge and online adaptive inferences (Florez *et al*. 2024).

Moerland et.al presents the through overview of model-based reinforcement learning, highlighting its novelty in integrating model learning and planning to improve decision-making efficiency (Moerland *et al*. 2023). Another study explored the use of deep learning models for structural health monitoring by detecting anomalies in acceleration data collected from cable-stayed bridges. Consequently, these models have proven effective in ensuring the safety and maintenance of large infrastructure by detecting subtle changes that could signal potential structural issues (Lee *et al*. 2024). The introduction of a preferences-based reinforcement learning techniques that uses preference instead of scalar rewards, with a tailored policy iteration algorithm. They conclude that this approach offers a robust alternative for handling of complex decision-making tasks where traditional methods are limited (Furnkranz *et al*. 2012, Fairbank and Alonso 2012). A comprehensive review of Monte Carlo Tree Search (MCTS) highlights its innovation in combining tree search with random sampling for decision-making in artificial intelligence. The study demonstrates MCTS effectiveness in handling complex decision processes and improving performance in areas like game play and planning (Browne *et al*. 2012). Nevertheless, an off-policy actor-critic algorithms designed for continuous action spaces, combining deterministic policy gradients with temporal difference learning, for efficient, scalable learning. Empirical evaluations on benchmark tasks show the algorithm superior performance over traditional methods (Degris *et al*. 2012, Silver *et al*. 2014). The integration of machine learning and k-nearest neighbors algorithms with Fuzzy Inference System (FIS) has been applied as adaptive controllers for earthquake characteristic-based control strategies in building structures subjected to wind and earthquake excitations. These methods demonstrate superior performance over traditional machine learning algorithms, significantly enhancing the seismic resilience of low- and mid-rise buildings (Ali *et al*. 2022, Bang *et al*. 2023, Naderpoor and Taghikhany 2022, Noureldin *et al*. 2021).

Numerous studies (Pisarski and Jankowski 2023, Eshkevari *et al*. 2023) embed a model-free policy-gradient DRL algorithms in a custom simulation environment to directly learn continuous actuator forces for active and semi-active buildings under harmonic and strong ground motions, optimizing structural control purely through trial-and-error without relying on prior system models. Deng *et al*. proposes a Deep Reinforcement Learning (DRL)-based control strategies called the Twin Delayed Deep Deterministic policy gradient (TD3) algorithm by augmenting the state representation with suspension dynamics and embedding physical safety constraints via guided training, immediate termination, and high penalties to yield control policies that are both safe and physically realizable within actuator limits (Deng *et al*. 2024).

Considering the aforementioned advantages of artificial intelligence techniques and research gap on control techniques, present investigation introduces an innovative approach by synergizing seismic characteristics prediction models with DRL to significantly enhance the performance and adaptability of a piezoelectric smart isolation system (PSIS). Therefore, using data from the Next Generation

Attenuation (NGA) project, seismic characteristics are analysed and classified into near-fault and far-field earthquakes. The DRL was deployed to optimize control strategies based on a sophisticated model of the PSIS. The DRL model undergoes rigorous training through the DDPG algorithm, utilizing a reward function designed for diverse control objectives under varying seismic conditions. Additionally, employing a FIS approach, facilitating customized seismic response control. Comprehensive numerical simulations with various earthquakes substantiate the effectiveness of the proposed techniques, establishing it as a promising solution to improve structural resilience against earthquakes.

2. Piezoelectric intelligent vibration isolation system

The piezoelectric smart isolation system comprises an advanced sliding vibration isolation mechanism and a sophisticated piezoelectric friction damper (PFD), as illustrated in Fig. 1. The PSIS is meticulously designed to deliver enhanced damping force by modulating the input voltage and precisely controlling the output force of a piezoelectric actuator, thereby adjusting the friction force exerted by the PFD at the interface. The specifications of the slide rail system include a stoke limit of ±15 cm (30 cm), a mass of 160 kg, a friction coefficient of 0.009, and a spring stiffness of 493 N/m. Additionally, the isolation platform has a mass of 10 kg. The intricate construction and fundamental principles of (1) the sliding vibration isolation mechanism and (2) the PFD are elaborated as follows:

(1) Sliding vibration isolation mechanism: The mechanism depicted in Fig. 1, primarily consists of a linear slider, linear rail, vibration isolation platform, and return spring, with the platform supporting the isolated object and the return spring providing the necessary return force. The linear rail offers a low-friction sliding surface, ensuring minimal resistance and promoting effective vibration isolation.

(2) Piezoelectric friction damper: The PFD consists of a damper base, piezoelectric actuator, friction rod, friction plate, and pre-pressurized bolts, with the bolts applying pre-pressure to create friction between the friction plate and actuator. When activated, the piezoelectric actuator exerts a controlled positive force on the friction plate, generating a precisely controlled sliding friction.

(3) When seismic disturbances affect the superstructure, friction is generated between the friction bar and friction plate due to relative motion, thereby altering the initial sliding friction of a damper.

2.1 Mathematical model of the PSIS

The comprehensive mathematical model of the PSIS is depicted in Fig. 2, illustrating that the PSIS framework comprises a sophisticated sliding isolation system and a PFD. Drawing upon the intricate mathematical model illustrated in Fig. 2, the motion equation has been formulated as follows

$$\begin{aligned} &\boldsymbol{M}\ddot{\boldsymbol{x}}(t) + \boldsymbol{C}\dot{\boldsymbol{x}}(t) + \boldsymbol{K}\boldsymbol{x}(t) \\ &= \mathbf{D}_2(u_d(t) + u_i(t)) + \boldsymbol{E}_1\ddot{x}_g(t) \end{aligned} \tag{1}$$

where $\ddot{x}(t)$, $\dot{x}(t)$ and $x(t)$ denotes the vectors of the acceleration, velocity and displacement; and $\ddot{x}_g(t)$ represents a surface acceleration induced by seismic forces. The M, C, and K correspond to mass, damping, and stiffness, respectively. Additionally, $\mathbf{D}_2$ and $\mathbf{E}_1$ represent the matrices that characterize the configuration of the control forces and the external forces. The term $u_i(t)$ refers to the friction experienced by the slider rail, while $u_d(t)$ represents the controlled friction obtained by the PFD. The vectors and matrices are described in Eq. (1) can be elucidated as follows

$$\begin{aligned} &\boldsymbol{x}(t) = \begin{Bmatrix} x_s(t) \\ x_b(t) \end{Bmatrix}, \quad \mathbf{D}_2 = \begin{Bmatrix} 0 \\ -1 \end{Bmatrix}, \\ &\mathbf{E}_1 = \begin{Bmatrix} -m_s \\ -m_b \end{Bmatrix}, \quad w(t) = \ddot{x}_g(t) \end{aligned} \tag{2}$$

$$\begin{aligned} &\boldsymbol{M} = \begin{bmatrix} m_s & 0 \\ 0 & m_b \end{bmatrix}, \quad \mathbf{C} = \begin{bmatrix} c_s & -c_s \\ -c_s & c_s \end{bmatrix}, \\ &\mathbf{K} = \begin{bmatrix} k_s & -k_s \\ -k_s & k_s + k_i \end{bmatrix} \end{aligned} \tag{3}$$

where m_s and m_b signify the mass of the superstructure and isolation layer; x_b and x_s denotes the displacements of the isolation layer and superstructure relative to the ground surface; k_i and μ_i denote the stiffness of the spring and friction coefficient of the linear rail within the sliding vibration isolation system, respectively. However, k_d and μ_d represent the stiffness and coefficient of friction of the PFD. The terms c_s and k_s signifies the damping and stiffness of the superstructure. If the parameter $u_d(t)$ in Eq. (1) is precisely zero, signifies the dynamic equation typical of

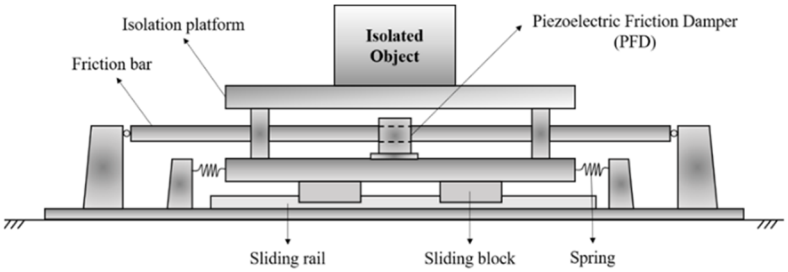

Fig. 1 Schematic representation of the PSIS structure

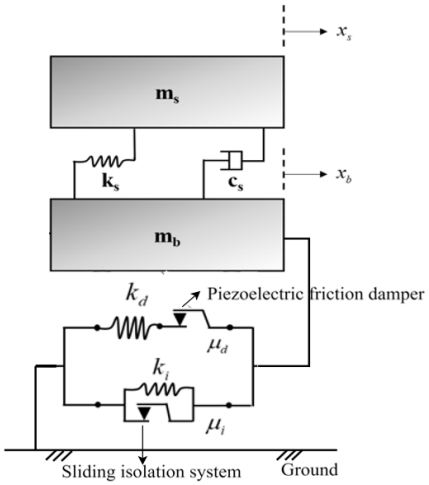

Fig. 2 Mathematical model of the PSIS

a conventional passive isolation system, commonly referred to as an uncontrolled isolation system. Then, Eq. (1) can be reformulated in the form of a first-order state-space representation as follows

$$\dot{\boldsymbol{z}}(t) = \boldsymbol{A}\boldsymbol{z}(t) + \boldsymbol{B}\,(u_d(t) + u_i(t)) + \boldsymbol{E}\,w(t) \tag{4}$$

where $\mathbf{z}(t)$ and $\dot{\boldsymbol{z}}(t)$ represent the state vectors, $\boldsymbol{A}$ represents the system matrix, $\boldsymbol{B}$ denotes the control force configuration matrix and $\boldsymbol{E}$ represents the external force configuration matrix after conversion. Upon expanding these aforementioned vectors and matrices, their explicit forms perhaps expressed as follows

$$\begin{aligned} &\boldsymbol{z}(t) = \begin{Bmatrix}\dot{\boldsymbol{x}}(t)\\ \boldsymbol{x}(t)\end{Bmatrix}, \quad \boldsymbol{A} = \begin{bmatrix}-\boldsymbol{M}^{-1}\boldsymbol{C} & -\boldsymbol{M}^{-1}\boldsymbol{K}\\ \boldsymbol{I} & \boldsymbol{0}\end{bmatrix},\\ &\boldsymbol{B} = \begin{bmatrix}\boldsymbol{M}^{-1}\boldsymbol{D}_2\\ \boldsymbol{0}\end{bmatrix}, \quad \boldsymbol{E} = \begin{bmatrix}\boldsymbol{M}^{-1}\boldsymbol{E}_1\\ \boldsymbol{0}\end{bmatrix}\end{aligned} \tag{5}$$

In this study, several assumptions have been integrated into the numerical simulation approach. First, the vertical deformation of the structure and its dynamic characteristics are considered to have negligible impact on the analysis and are thus disregarded. Second, the friction behavior of the PFD damper and lateral movement follows Coulomb's law, maintaining a constant coefficient of friction throughout the motion. Third, the coefficient of kinetic friction is assumed to be the same as the static friction coefficient. In the continuous-time application of the PSIS, the process involves converting to discrete time. In the discrete-time domain, the temporal progression at the k^{th} step is given by $t = k\Delta t$, where Δt represents the incremental time step used for numerical integration. Additionally, both the control force and the seismic disturbance force are treated as constants during each integration step Δt. The formulation within this discrete-time framework is developed as follows

$$\begin{aligned} &u_d(t) = u_d[k],\ \ u_i(t) = u_i[k],\ \ w(t) = w[k]\\ &\text{for} \quad k\Delta t \le t < (k+1)\Delta t\end{aligned} \tag{6}$$

The attainment of a standardized solution within the discrete time domain necessitates integrating the discrete - time representation of Eq. (6) in Eq. (5), resulting in

$$\boldsymbol{z}[K+1] = \boldsymbol{A}_d\,\boldsymbol{z}[K] + \boldsymbol{B}_d(u_d[K] + u_i[K]) + \boldsymbol{E}_d\,w[K] \tag{7}$$

where $\mathbf{A}_d$, $\mathbf{B}_d$, and $\mathbf{E}_d$ serving as the system correlation matrices of A, B, and E, respectively, in the discrete time domain, are delineated as follows

$$\begin{aligned} &\mathbf{A}_d = e^{\mathbf{A}\Delta t}; \quad \mathbf{B}_d = \mathbf{A}^{-1}(\mathbf{A}_d - \mathbf{I})\mathbf{B};\\ &\mathbf{E}_d = \mathbf{A}^{-1}(\mathbf{A}_d - \mathbf{I})\mathbf{E}\end{aligned} \tag{8}$$

If the values of $u_d\,[k]$ and $u_i\,[k]$ are known during the k_{th} iteration, the discrete time formulation of Eq. (7) was utilized to determine the complete state responses of the system in a $z[k+1]$ step. Nevertheless, the nonlinear forces attributed to both the PFD damper friction $u_d\,[k]$ and the rail friction $u_i\ [k]$ impede the direct measurement, these nonlinear characteristics can be rigorously expressed as follows

$$u_d[k] = min(\,|\tilde{u}_d[k]|\,, u_{d,max}[k])\; sgn(\,\tilde{u}_d[k]) \tag{9}$$

$$u_i[k] = min(\,|\tilde{u}_i[k]|\,, u_{i,max}[k])\; sgn(\tilde{u}_i[k]) \tag{10}$$

$$\begin{aligned} &\tilde{u}_d[k] = k_d\ \mathrm{D}(z[k]\text{-}z[\mathrm{k}\text{-}1])+\mathrm{u}_d[k-1];\\ &\tilde{u}_i[k] = G_z z[k] + G_u u_d[k] + G_w w[k]\end{aligned} \tag{11}$$

$$u_{d,max}[k] = \mu_d\,N[k] = \mu_d(N_0 + C_z\,V[k]) \tag{12}$$

where $u_{d,max}[k]$ signifies the maximum static coefficient of friction of damper, while $u_{i,max}[k]$ represents a maximum rail friction coefficient and C_z is the piezoelectric actuation coefficient. The configuration matrix D is defined as [0 0 0 1], and G_u is set to -1. Subsequently, the terms $G_z$and G_w are defined as follows

$$\begin{aligned} &G_z = -(D_1B_d)^{-1}(D_1A_d),\\ &G_w = -(D_1B_d)^{-1}(D_1E_d)\end{aligned} \tag{13}$$

where the configuration matrix D_1 = [0 1 0 0]. Finally, the calculated values of $u_d[k]$ and $u_i[k]$, derived from Eqs. (9) and (10) respectively, are subsequently incorporated to Eq. (7), thus allowing the evolution of the system response in the subsequent step. Furthermore, the analytical simulation technique effectively replicates the PSIS response throughout the earthquake time history. Effectiveness is achieved through an iterative computation of the responses of the system until the entire time history is comprehensively resolved. Furthermore, the Non-sticking friction (NSF) controller draws inspiration from the anti-lock braking system to prevent wheel lock-up during emergency braking, thereby maintaining vehicle control and enhancing safety (Lu *et al*. 2011). This system operates on principles akin to those of controlled friction dampers used in vibration isolation systems which gives the positive force that can be applied to the piezo actuator. The positive force can be obtained from the following equation

$$N(t) = N_{max}\,tanh(\,\beta|\dot{x}_b(t)|) \tag{14}$$

where β is the velocity adjustment factor, $\dot{x}_b(t)$ is the sliding velocity of isolation platform, Eq. (14) is the NSF controller applied in this study. Furthermore, if the presence of preload in the friction damper is considered, the above

equation should be modified to the following equation

$$N(t) = N_0 + N_{max}\, tanh(\beta|\dot{x}_b(t)|) \tag{15}$$

By comparing Eq. (14) with $N(t) = N_0 + C_z V(t)$, the NSF controller for the piezoelectric drive voltage can be obtained and expressed as follows

$$V(t) = V_{max}\, tanh(\beta|\dot{x}_b(t)|) \tag{16}$$

where V_{max} is the maximum supply voltage and its relationship to the supply voltage is $V_{max} = N_{\max} / C_z$. While it is evident that a higher value, the more sensitive $tanh$ function is to change. Finally, Eq. (16) is the voltage of the PFD adopted in this study. The determination of the necessary drive voltage of the PFD in real-time solely involves obtaining the relative velocities with respect to the isolation layer.

3. Deep deterministic policy gradient model

The deep deterministic policy gradient model is a RL algorithm specially designed for environments that feature continuous action spaces. By integrating actor-critic methods, the actor learns the policy while the critic evaluates the actions, optimizing decision-making processes. DDPG employs neural networks for function approximation and utilizes experiences replay to enhance stability and learning efficiency in DRL applications. Given its capability to handle continuous action spaces and to significantly improve the effectiveness of the control system in determining an optimal control parameter, particularly the velocity adjustment factor β for near-fault and far-field earthquakes with varying seismic characteristics, this study introduces the DDPG algorithm.

This innovative approach aims to develop an intelligent seismic characteristic control module, as depicted in Fig. 3, that can adapt to a wider range of seismic scenarios and optimizing response strategies. The DRL model is particularly valuable in seismic characterisation control due to its exceptional ability to navigate complex and dynamic environments. Its primary goal is to meticulously analyse measured seismic time-series data to determine the ideal control parameters necessary for stabilizing the system in anticipation of the main seismic events. Furthermore, the DRL model is instrumental in producing detailed two-dimensional distribution maps based on refined seismic data, further aiding in the optimization of response strategies across a broad range of seismic characteristics.

As mentioned earlier, the DDPG algorithm is a continuous-action method within DRL family, is employed to train specialized control modules for a PSIS under both near-fault and far-field earthquake conditions. The optimal control parameter β is mapped to seismic features specifically the Near-Far Characteristic ratio (NF-ratio) and Peak Ground Acceleration (PGA) by partitioning their two-dimensional distribution into discrete blocks, each corresponding to a distinct seismic ranges. During training, the DDPG agent explores β values within specified ranges using its actor-critic architecture: the actor networks suggest optimal β values, and the critic network evaluates them with a reward function that measures reductions in isolation layer displacement and superstructure acceleration relative to passive control. Extensive training of the DRL model undergoes to identify optimal control parameters for various seismic blocks, which are then applied to the fuzzy inference system.

3.1 LSTM Seismic characteristics prediction module

The present investigation integrates the Long Short-Term Memory (LSTM) neural networks prediction model to classify the characteristics of the near-fault or far-field earthquakes by analyzing the first three seconds of seismic waveforms. These LSTM networks are particularly suitable for this task due to their ability to process sequential data and capture long-term dependencies, which are essential for accurate earthquake classification. Unlike traditional classifiers such as support vector machines or random forests (Berhich *et al.* 2023), which may struggle with sequential data without extensive feature engineering, LSTM models can automatically learn relevant features from raw time-series seismic data. This ability makes LSTM models more efficient and adaptable, providing superior performance in earthquake prediction tasks compared to other machine learning algorithms. The ground motion data used in this investigation was selected from the comprehensive NGA ground motion project (Dolce *et al.* 2000). To ensure precision, a comprehensive database was chosen, consisting of a total of 1652 recorded earthquakes.

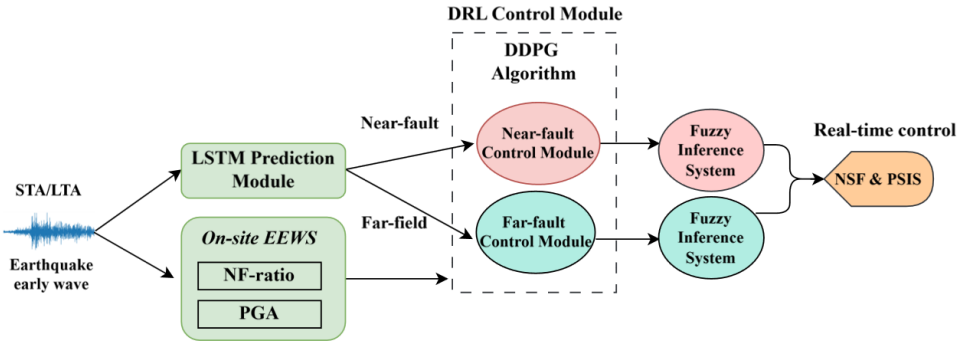

Fig. 3 Schematic diagram of the intelligent DRL seismic characteristics control model

This dataset includes 754 near-fault and 898 far-field earthquakes. Typically, the determination of the earthquake arrival time depends on the application of the short-term average (STA) and long-term average (LTA) criteria, often referred to as the STA/LTA ratio.

Upon determining the earthquake events utilizing the STA/LTA ratio, the horizontal initial waveforms are sampled at 50 Hz, yielding 151 data points which are then input into the model and pre-processed. Initially, the inputs data length is 151, with an embedding layer reducing training data dimension from 402 to 10 neurons, subsequently connecting to the LSTM layer. The LSTM architecture consists of an embedding layer followed by two hidden layers employing ReLU activation functions, and a final fully connected layer utilizing a sigmoid function for dichotomous output. Finally, to employ LSTM for near-fault and far-field earthquake prediction, the label value is set to 0 and 1. The prediction model aims to dichotomize characteristics of earthquakes, utilizing the binary cross entropy (BCE) as its loss function, which is computed in the following

$$\psi_E = -\frac{1}{N}\sum_{i=1}^{N} \mathcal{Y}_i \times log(\hat{\mathcal{Y}}_i) + (1-\mathcal{Y}) \times log(1-\hat{\mathcal{Y}}_i) \quad (17)$$

here $\mathcal{Y}_i$ represents an actual target value, $\hat{\mathcal{Y}}_i$ denotes the neural network output, and N is the number of test samples. For training and testing, 1652 earthquakes from the seismic database are utilized, with 80% randomly selected for training and 20% for testing. Consequently, near-fault earthquakes are labelled 1 and far-field earthquakes as 0. The training was conducted over 80 epochs, using 1320 samples for training and 332 samples for testing, with accuracy and loss indices as the convergence criteria parameters. As a result, the type of earthquakes obtained are 134 near-fault and 11 far-field earthquakes, demonstrating the model accuracy in discerning between near-fault and not-near-fault earthquakes, achieving an accuracy of 94.27%, a precision of 94.36%, a recall of 92.41%, and an F1-score of 93.38%. Additionally, the LSTM seismic characteristic prediction module performs well in distinguishing between near-fault and far-field earthquake scenarios.

The inappropriate selection of the control parameter of the velocity adjustment factor β can result in high-frequency responses in the superstructure, undermining the ineffectiveness of the isolation system. Additionally, it is impractical to achieve optimal control with a single control parameter across varying characteristics and magnitudes of seismic waves. Consequently, this study analyses the parameters of various earthquakes to identify a range of parameters suitable for different seismic characteristics. Therefore, the present study introduces the DRL control modules for both the seismic domains. The DRL model uses quantitative indexes like as the PGA and the NF-ratio to classify the near-fault and far-field earthquakes more accurately. This classification intent to identify a corresponding control parameter to achieve optimal control.

3.2 DRL seismic characteristics control module

The DRL seismic motion characteristics control module uses the Near-Far (NF) characteristics ratio and the PGA as input to the model, yielding the optimal parameter β as output. These PGA values are predicted using six parameters: absolute acceleration (P_a), absolute velocity (P_v), absolute displacement (P_d), effective predominant period (τ_c), integral of squared velocity (*IV2*), and cumulative absolute velocity. In the context of the near-fault earthquakes, these parameters are chosen as 0.1769, 6.7413, 2.6831, 3.9576, 50.984, and 0.1023 for P_a, P_v, P_d, τ_c, IV2, CAV, respectively.

Similarly, in the case of far-field earthquakes, these parameters chosen as 0.0374, 1.5630, 0.6138, 4.0131, 1.5872, and 0.0247 for the respective parameters. Additionally, two more parameters horizontal high frequency cumulative acceleration energy $(C_{Ea})_{\text{horizontal}}$ and horizontal high frequency cumulative velocity energy $(C_{Ev})_{\text{horizontal}}$ are included, making a total of eight index parameters used as NF ratio functions (Hsu *et al*. 2013). These parameters are calculated by performing a Fast Fourier Transform (FFT) on the first three seconds of arrival waves. The $(C_{Ea})_{\text{horizontal}}$ and $(C_{Ev})_{\text{horizontal}}$ parameters are selected as 0.0209 and 0.9708 for the near-fault earthquakes, and 0.0039, 0.1249 for the far-field earthquakes. The NF-ratio is expressed as follows

$$NF-\text{ratio} = \sum_{i=1}^{8} \left\{ \left[\frac{x_i}{\left(\frac{\overline{x_{iN}} + \overline{x_{iF}}}{2} \right)} \right] \times \frac{\overline{x_{iN}}}{\overline{x_{iF}}} \right\} \quad (18)$$

where $x_1 = P_a,\ x_2 = P_v,\ x_3 = P_d,\ x_4 = \tau_c,\ x_5 = IV2,\ x_6 = CAV,\ x_7 = (C_{Ea})_{\text{horizontal}},\ x_8 = (C_{Ev})_{\text{horizontal}}$. The $\overline{x_{iN}}$ and $\overline{x_{iF}}$ are the average values of all near-fault and far-field earthquakes in the seismic database, while the NF-ratio is selected as 9.4968 and 3.8355 for the near-fault and far-field earthquakes, respectively. An initial preload of 100 N is selected for near-fault and far-field earthquake control modules.

The study establishes a relationship between the control parameter β and the distribution of near-fault and far-field earthquakes by dividing the two-dimensional distribution maps into specific blocks based on the NF-ratio and Peak Ground Acceleration (PGA), as shown in Figs. 4 and 5. The distribution of optimal control parameters is highly dispersed, indicating that there is no obvious trend. For near-fault earthquakes, the map is divided into 12 blocks with four horizontal and three vertical divisions, each representing different ranges of NF-ratio and PGA. These blocks are then used as inputs to a DRL model, which determines the optimal control parameter β for each block by balancing the acceleration and displacement responses to optimize structural control under varying seismic conditions. A similar approach is applied to far-field earthquakes, resulting in six blocks with three horizontal and two vertical divisions. The training data for the near-fault control module is derived from the data shown in Fig. 4(b). Excluding blocks (L, I) and (S, IV), the seismic time-history data for the remaining blocks are stored in their

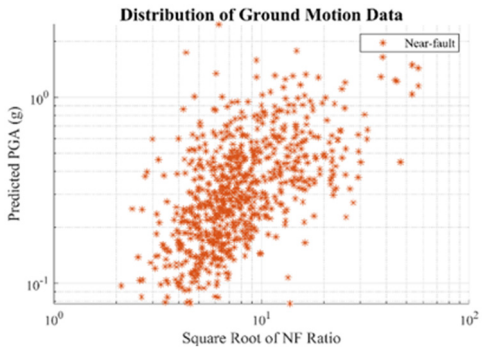

(a) 2-dimensional map of earthquakes

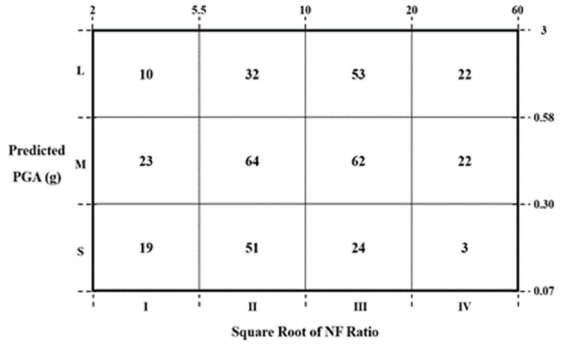

(b) Selected data in each block

Fig. 4 Distribution of near-fault earthquake ground motions

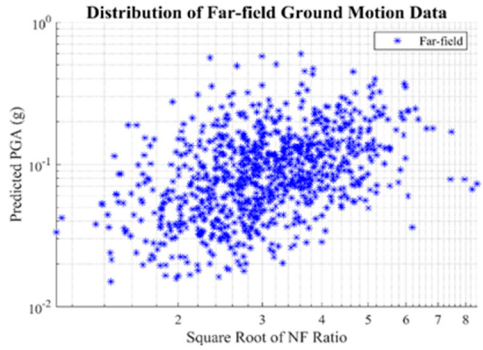

(a) 2-dimensional map of earthquakes

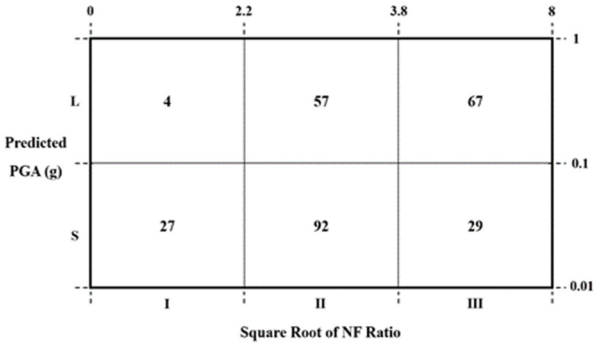

(b) Selected data in each block

Fig. 5 Distribution of far-field earthquake ground motions

corresponding folders. In each sample round, the step function and reset function are executed, with the agent selecting a β-value between 0 and 100 for the current iteration. This value is then stored in the (M, II) block in the environment as an array for reward value calculation. The near-fault seismic reward function, R_{NF} is expressed as follows

$$R_{NF} = \frac{D_{\text{passive}} - D_i}{D_{\text{passive}} - D_{min}} \tag{19}$$

where D_{passive} represents the maximum displacement of the isolation layer under passive control, D_i is the maximum displacement under NSF control with the selected β-value, and D_{min} is the smallest maximum displacements of isolation layer when β is set to 1, 2, 3, and 100. Eq. (19) employs the concept of Min-Max normalization to ensure that the output reward value falls between 0 and 1, effectively quantifying the difference between the β selected by the agent and the actual optimal β. When D_i is closer to D_{min}, the reward value for those round approaches 1. By applying Eq. (19) to calculate the incentive values for each of the 64 near-fault earthquakes, R1, R2, R3, and R64 are obtained. To minimize the influence of the extreme values, the average of these 64 R-values, denoted as R_{avg}, is used as the incentive value for current round in block (M, II). Similarly, the training data for the far-field control module is derived from selected seismic data shown in Fig. 5(b). The DRL environment settings, step function and reset function of the far-field control module are the same as that of the near-fault control module, with the primary being that the agent in the step function selected β-values between 0.1 to 19.9 for each iteration during training. Additionally, the reward function in the far-field control module is designed with the primary objective of minimizing the acceleration response of the superstructure while ensuring that the isolation layer displacement does not exceeds the 15 cm limit. The reward function, R_{FF} is defined as follows

$$R_{FF} = \begin{cases} \dfrac{A_{max} - A_i}{A_{max} - A_{min}}, & \text{if } D_{\text{passive}} < 15 \text{ cm} \\ \dfrac{A_{max} - A_i}{A_{max} - A_{min}} + 2 \times \dfrac{D_{\text{passive}} - D_i}{D_{\text{passive}} - D_{min}}, & \text{if } D_{\text{passive}} \geq 15 \text{ cm} \end{cases} \tag{20}$$

where A_{max} is the maximum of the peak superstructure accelerations for β-values 0.1, 0.2, 0.3 and 19.9; $A_{min}$is the minimum of these peak accelerations and A_i is the peak acceleration of the superstructure for the selected β-value of each round of the NSF control. The average value, R_{avg} of each block is then computed and used as the incentive value for that block in the given round. The optimal control

parameters for far-field blocks are determined using a DRL model with a set output range of 0 to 20, When data is insufficient, parameters from adjacent blocks are averaged to ensure effective control. Consequently, the far-field earthquake control module prioritizes reducing acceleration responses while maintaining comfort and usability, ensuring that the displacement of the isolation layer remains within acceptable limits.

Optimizing the β parameter is essential for effective seismic isolation and damping, as it governs the control system ability to mitigate structural displacement and acceleration under earthquake excitation. By tailoring β to specific seismic characteristics, the isolation system maintains consistent performance across varying conditions and adapts in real time. This optimization significantly improves overall system efficiency, reduces structural damage, and keeps isolation layer displacements within prescribed safety thresholds. These optimal parameters are obtained using the DDPG algorithm in the subsequent sections.

3.3 Deep deterministic policy gradient algorithm

In the present study, the Deep Deterministic Policy Gradient (DDPG) algorithm employs for its proficiency in handling continuous action spaces, which is crucial for optimizing control parameters in seismic characterization control modules. As a model-free reinforcement learning algorithm, DDPG is selected due to its effectiveness in optimizing control policies within complex environments, such as those involving near-fault and far-field seismic data distributions. The actor-critic architecture of DDPG enhances the learning process by maximizing reward functions tailored to specific seismic control objectives. The DDPG algorithm incorporates four neural network models: actor network, critic network, critic target network, and actor target network. In this study, these models are constructed using Keras, a Python library valued for its user-friendly interface, modular design, and scalability. The architecture of the actor neural network, as shown in Fig. 6, comprised of an input layer that processes observed states, varying in scale according to the amount of seismic data per block. It has two hidden layers with 600 and 300 neurons, both using ReLU activation functions, and an output layer with a single neuron using a *tanh* activation function.

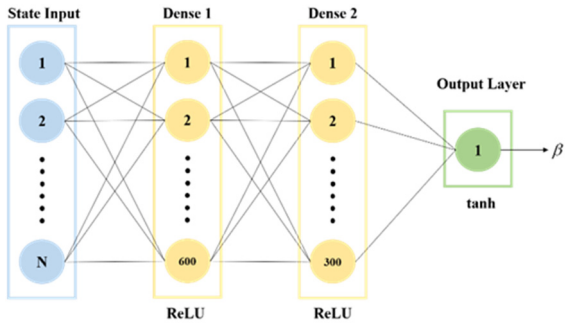

Fig. 6 Actor neural network architecture diagram

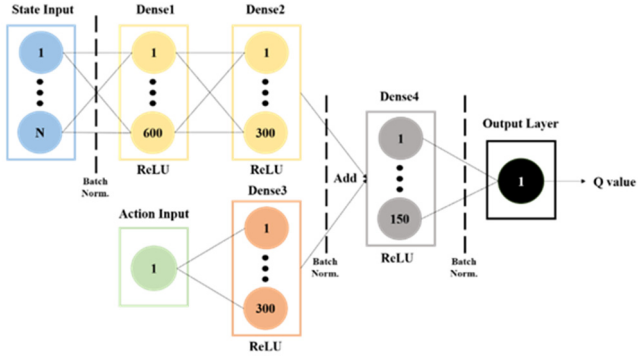

Fig. 7 Critic neural network architecture diagram

The critic neural network, illustrated in Fig. 7, assesses the actions of the actor to guide decision-making. It consists of two input layers: the first receives the observed state and connects to two fully connection layers with 600 and 300 neurons, while the second receives the action value β from the actor and connects to a fully connection layer with 300 neurons. The outputs of these layers are combined and passed through a fully connection layer with 150 neurons, with the final output layer producing a Q-value that represents the action score under the observed state,utilizing ReLU functions for all fully connected layers. The pseudo code of the DDPG algorithm training process, highlighting the modification of the critic network's loss function from Mean Squared Error (MSE) to Mean Absolute Error (MAE) to speed up training is illustrated in Fig. 8.

The DDPG is a learning-based algorithm that extends the Actor-Critic (AC) architecture to continuous action spaces. Unlike Deep Q-Networks (DQN) (Mnih *et al.* 2015), which struggle with continuous actions, DDPG leverages two key concepts from DQN: experience replay and fixed target networks. This allows DDPG to stabilize learning and achieve end-to-end policy learning across various tasks, as demonstrated in multiple simulation environments. In a typical reinforcement learning configuration, the environment is engaged by an agent in discrete time intervals.

The observation x_t received by the agent at time t, an action m_t is taken, and a reward r_t is obtained. The state $\mathscr{b}_t$ can be defined as $\mathscr{b}_t = (x_1, m_1, \ldots, m_{t-1}, x_t)$ assuming a fully observable environment. The policy π, which maps states to actions, is characterized by $\pi: \mathcal{S} \rightarrow \mathcal{P}(\mathcal{A})$, where $\mathcal{S}$ denotes the state space and $\mathcal{A} = (\mathbb{R}^N)$ represents the action space. The objective of the DDPG algorithm is to increase the expected returns of performance objective function, which aggregates discounted forthcoming rewards

$$R_t = \sum_{i=t}^{T} \gamma^{(i-t)} r(\mathscr{b}_i, m_i) \tag{21}$$

where γ represents the discount factor which are chosen to $\gamma \in [0,1]$. The expected return of action a_t in state $\mathscr{b}_t$ is governed by policy π, is encapsulated by the action value function $Q^{\pi}(\mathscr{b}_t, m_t)$.

$$Q^{\pi}(\mathscr{b}_t, m_t) = \mathcal{M}_{r_{i \geq t}, \mathscr{b}_{i>t} \sim E, m_{i>t} \sim \pi}[R_t | \mathscr{b}_t, m_t] \tag{22}$$

Algorithm 1 DDPG algorithm

Randomly initialize critic network $Q(s,a|\theta^Q)$ and actor $\mu(s|\theta^\mu)$ with weights θ^Q and θ^μ.
Initialize target network Q' and μ' with weights $\theta^{Q'} \leftarrow \theta^Q$, $\theta^{\mu'} \leftarrow \theta^\mu$
Initialize replay buffer R
for episode = 1, M **do**
  Initialize a random process $\mathcal{N}$ for action exploration
  Receive initial observation state s_1
  for t = 1, T **do**
    Select action $a_t = \mu(s_t|\theta^\mu) + \mathcal{N}_t$ according to the current policy and exploration noise
    Execute action a_t and observe reward r_t and observe new state s_{t+1}
    Store transition (s_t, a_t, r_t, s_{t+1}) in R
    Sample a random minibatch of N transitions (s_i, a_i, r_i, s_{i+1}) from R
    Set $y_i = r_i + \gamma Q'(s_{i+1}, \mu'(s_{i+1}|\theta^{\mu'})|\theta^{Q'})$
    Update critic by minimizing the loss: $L = \frac{1}{N}\sum_i (y_i - Q(s_i, a_i|\theta^Q))^2$
    Update the actor policy using the sampled policy gradient:

$$\nabla_{\theta^\mu} J \approx \frac{1}{N}\sum_i \nabla_a Q(s,a|\theta^Q)|_{s=s_i, a=\mu(s_i)} \nabla_{\theta^\mu}\mu(s|\theta^\mu)|_{s_i}$$

    Update the target networks:

$$\theta^{Q'} \leftarrow \tau\theta^Q + (1-\tau)\theta^{Q'}$$
$$\theta^{\mu'} \leftarrow \tau\theta^\mu + (1-\tau)\theta^{\mu'}$$

  end for
end for

Fig. 8 Pseudo code of the DDPG algorithm

Using the Bellman equation, this can be recursively defined as

$$Q^\pi(\mathscr{b}_t, m_t) = \mathcal{M}_{r_t, \mathscr{b}_{t+1}\sim E}[r(\mathscr{b}_t, m_t) + \gamma \mathcal{M}_{m_{t+1}\sim\pi}[Q^\pi(\mathscr{b}_{t+1}, m_{t+1})] \quad (23)$$

For deterministic policies, the action-value function simplifies to

$$Q^\mu(\mathscr{b}_t, m_t) = \mathcal{M}_{r_t, \mathscr{b}_{t+1}\sim E}[r(\mathscr{b}_t, m_t) + \gamma Q^\mu(\mathscr{b}_{t+1}, \mu(\mathscr{b}_{t+1}))] \quad (24)$$

Further, the DDPG employs a parametric actor function $\mu(\mathscr{b}|\theta^\mu)$ to determine actions and a critic function $Q(\mathscr{b}, m|\theta^Q)$ to evaluate them. The actor parameters are updated using the policy gradient

$$\nabla_{\theta^\mu} J \approx \mathcal{M}_{\mathscr{b}_t\sim\rho^\beta}\left[\nabla_{\theta^\mu} Q(\mathscr{b}, m|\theta^Q)|_{\mathscr{b}=\mathscr{b}_t, m=\mu(\mathscr{b}_t|\theta^\mu)}\right] = \mathcal{M}_{\mathscr{b}_t\sim\rho^\beta}\left[\nabla_m Q(\mathscr{b}, m|\theta^Q)|_{\mathscr{b}=\mathscr{b}_t, m=\mu(\mathscr{b}_t)} \nabla_{\theta_\mu}\mu(\mathscr{b}|\theta^\mu)|_{\mathscr{b}=\mathscr{b}_t}\right] \quad (25)$$

To stabilize learning, DDPG uses a replay buffer to store transitions and samples mini-batches for updates. It also employs target networks for both actor and critic, updated softly

$$\theta' \leftarrow \tau\theta + (1-\tau)\theta' \quad (26)$$

where $\tau << 1$ and θ' represents the parameter of the target network, θ represents the original network parameter. Then the batch normalization is applied to handle different physical units and ensure efficient learning. For exploration, DDPG adds noise to the policy using the Ornstein-Uhlenbeck process (Uhlenbeck and Ornstein 1930)

$$\mu'(\mathscr{b}_t) = \mu(\mathscr{b}_t|\theta_t^\mu) + \mathcal{N} \quad (27)$$

The optimal parameters for each earthquake data block, whether in near-fault or far-field control environment, are determined through the parameter β within the DDPG model. The model includes 10 training blocks (yellow colour) for near-fault environments and 5 for far-field environments.

The convergence of average reward value, actor loss, and critic loss typically occurs after approximately 600 training iterations in both control modules. For the blocks (S, I), (S, II), (S, III), (M, I), (M, II), (M, III), (M, IV), (L, II), (L, III) and (L, IV) the optimal β values are 25.6, 44.3, 65.5, 37.8, 62.9, 88.7, 99.8, 57.3, 76.8, and 87.5, respectively are achieved after approximately 1000 iterations. Additionally, due to the insufficient seismic data in blocks (L, I) and (S, IV), the control parameters for block (L, I) are averaged from the control parameters of (M, I), (M, II), and (L, II), resulting in a of 52.7. Similarly, the value for (S, IV) is averaged from (S, III), (M, III), and (M, IV) control parameters, resulting in a value of 84.7. These distributions of the optimal control parameters are illustrated in Fig. 9(a).

Similarly, the value for (S, IV) is averaged from (S, III), (M, III), and (M, IV) control parameters, resulting in a value of 84.7. These distributions of the optimal control parameters are illustrated in Fig. 9(a). In the context of far-field earthquakes over 1000 iterations, the optimal parameter β values are achieved as 8.1, 10.6, 15.1, 16.5, and 19.9 for the (S, I), (S, II), (S, III), (L, II), and (L, III) earthquakes blocks, respectively, converging at 300 iterations. However, the value for the (L, I) block is too small, so the control parameter is taken as the average of (S, I), (S, II), and (L, II), resulting in 11.7. These optimal trends are illustrated in Fig. 9(b). It is evident from these figures that blocks in far-field domains exhibit more fluctuations in the training trend compared near-fault blocks due to a weaker and more complex reward function. This underscores the necessity of designing appropriate reward functions for effective parameter optimization in deep reinforcement learning. This capability ensures that the derived control parameters are suitable for real-time application in fuzzy logic inference systems, thereby

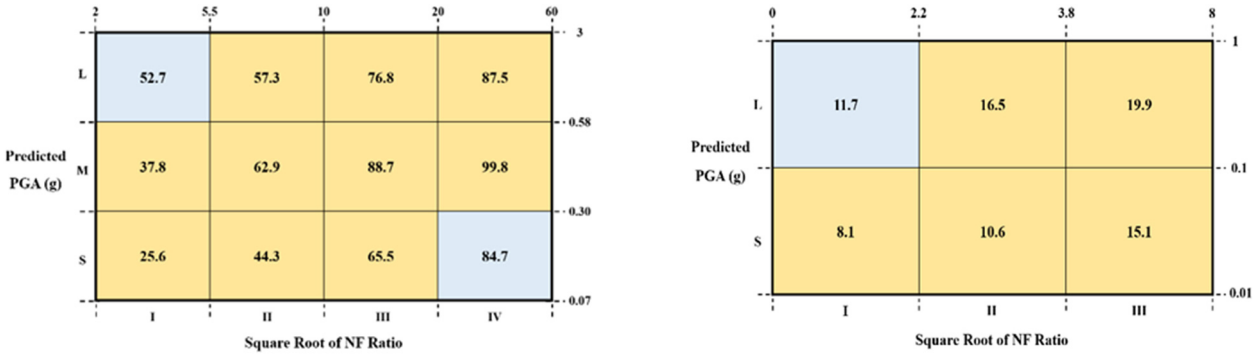

(a) Near-fault earthquakes (b) Far-field earthquakes

Fig. 9 Distribution of optimal parameter β in each block for both earthquakes

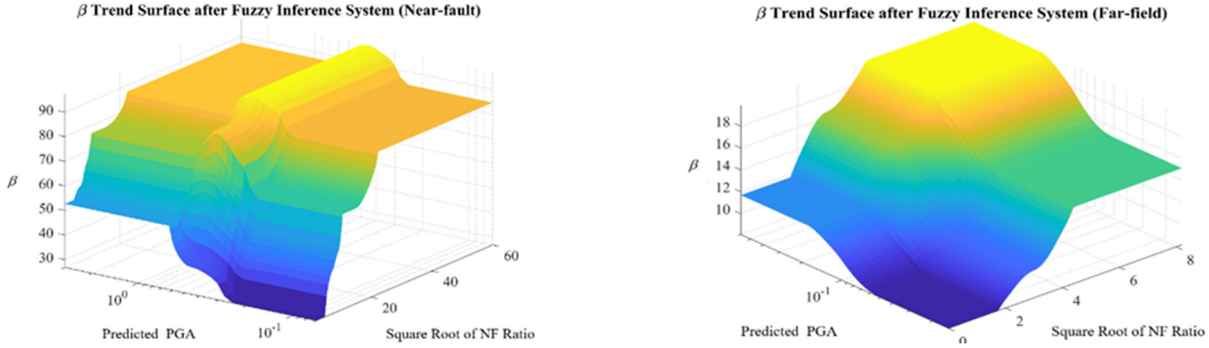

(a) For near-fault earthquakes (b) For far-field earthquakes

Fig. 10 Surfview relation between inputs and output of the FIS

improving the system response to seismic activities. In addition to variation of the control parameter β in each block for both near-fault and far-field earthquakes, the study integrates the Mamdani-FIS to determine the real time control parameter based on changes in PGA and NF-ratio for both types of earthquakes. These variations are depicted in Fig. 10. This approach enables the development of an intelligent seismic isolation and damping system capable of dynamically determining the optimal control parameter β in real time, thus adapting to varying seismic characteristics.

The DDPG algorithm proves to be highly effective for the present investigation due to its ability to handle continuous action spaces, which is essential for optimizing control parameters in seismic characterization control modules. As a model-free algorithm, DDPG is particularly well-suited for the complex environments associated with near-fault and far-field seismic data distributions. Its actor-critic architecture enhances the learning process by optimizing of control policies through tailored reward functions specific to seismic control objectives. Its modular design and scalability add to the algorithm effectiveness. The DDPG's ability to adjust the β control parameter across different seismic data blocks, both near-fault and far-field, demonstrates its capability to fine-tune control strategies effectively. The convergence of reward values, actor loss, and critic loss after approximately 600 training iterations further underscores the algorithm efficiency in learning and applying optimal control parameters. Additionally, DDPG algorithm employs fixed target networks, and noise addition via the Ornstein-Uhlenbeck process (Uhlenbeck and Ornstein 1930), which stabilizes learning and ensures consistent policy development across various tasks. This stability is particularly important in managing the fluctuating conditions in seismic environments, especially in far-field earthquake scenarios where the reward function is more complex and less stable. Due to these advantages its adaptability to continuous action spaces, its robust learning mechanisms, and real-time optimization of control parameters DDPG is well-suited for this study, as verified through numerical simulations. Furthermore, its integration with fuzzy inference system enhances the system response to seismic activities, making DDPG a powerful tool for developing intelligent seismic isolation and damping systems.

4. Numerical simulations and results discussions

The numerical simulations are meticulously performed to evaluate the efficacy of the PSIS control system in attenuating structural responses under the near-fault and far-field earthquakes. These simulations utilized the optimal parameters of the velocity adjustment factor β and the preload N_0. The specific structural characteristics considered are detailed in Table 1. The responses are rigorously compared against those of passive control, a Deep Deterministic Policy Gradient model designed for Near-fault (DDPG-NF) control, and various sophisticated

Table 1 Structural characteristics utilized for the PSIS numerical simulation

Superstructure		Isolation system		PFD	
Superstructure mass (m_s)	20 kg	Isolation stiffness (k_i)	1000 N/m	Damper friction coefficient (μ_d)	0.07
Isolation platform mass (m_b)	140 kg	Time period (ω_i)	0.41 Hz	Damper stiffness (k_d)	10^6 N/m
Natural frequency (ω_s)	2.04 Hz	Slide friction coefficient (μ_i)	0.009	Actuation force coefficient (C_z)	0.5 N/V
Damping ratio (ξ)	1.5%			Initial pre-load (N_0)	100 N

fuzzy control strategies (fuzzy12345, fuzzy13555, and fuzzy15555) (Lu *et al*. 2010). These fuzzy control strategies are distinct fuzzy logic-based algorithms applied in a PSIS for controlling the system response during the near-fault and far-field seismic events. The fuzzy 15555, inspired by anti-lock braking systems, employs five discrete input and output membership levels, and triggers an abrupt increase to the maximum voltage as soon as any relative motion is detected, thereby delivering a rapid, high-force response that effectively suppresses large displacements and accelerations during earthquake events. The fuzzy 13555 controller retains the five-level structure but moderates its low-velocity response by limiting the driving voltage to an intermediate level when sliding velocity is small, resulting in a more gradual voltage increase and reduced sensitivity under those conditions. The fuzzy 12345 controller, akin to a proportional control strategy in which the output voltage scales linearly across five membership functions in direct proportion to the measured velocity. This produces a smooth, continuous voltage ramp that is particularly well-suited to mild or moderate ground motions where abrupt force jumps are unnecessary and could degrade ride comfort or introduce high-frequency structural loads. Fundamentally, the key difference lies in the intensity of the control strategy, with fuzzy 15555 offering the fastest response, fuzzy 13555 being more moderate, and fuzzy 12345 providing a smoother, proportional control. Each controller is suited for different seismic conditions, with fuzzy 15555 being the most effective in reducing isolation later displacement and improving isolation performance, especially in near-fault earthquakes.

The initial pre-load N_0 value set to 100 N for both earthquakes. The near-fault and far-field earthquakes selected for evaluation are distinctly different from those used in the design and training database of the controllers, as detailed below:

(i) El Mayor-Cucapah earthquake (2010), station: Michoacan de Ocampo, peak acceleration: 5.2719 m/s^2 (0.538 g), PEER database (near-fault)

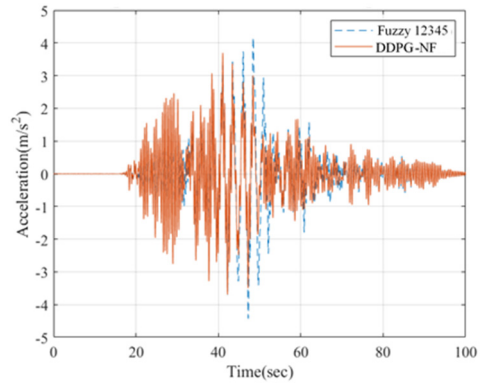

(a) Superstructure acceleration

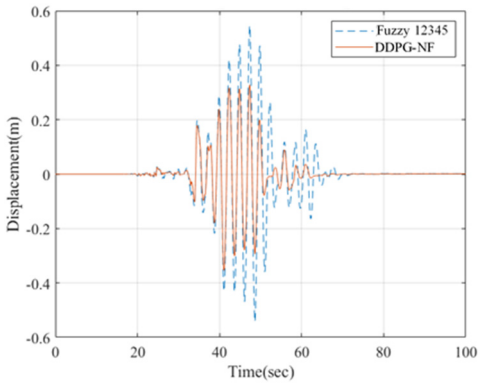

(b) Isolation layer displacement

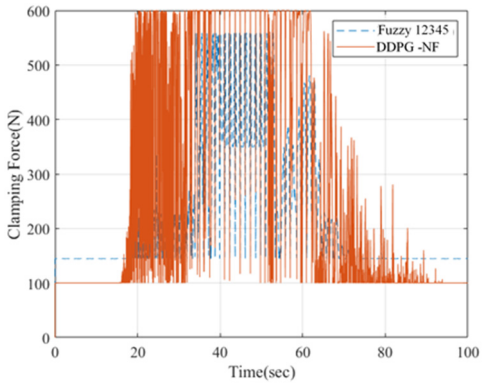

(c) PFD clamping force

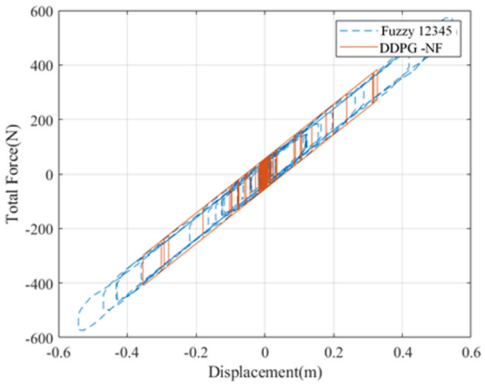

(d) Hysteresis loop

Fig. 11 Response comparison between fuzzy12345, DDPG-NF controller under near-fault EI Mayor-Cucapah earthquake

Table 2 Response comparison of various controllers for near-fault EI Mayor-Cucapah earthquake

Control system	Superstructure		Isolation layer	
	Acceleration (m/s^2)	Displacement (m)	Acceleration (m/s^2)	Displacement (m)
Passive	6.7472 (1.000)	1.0424 (1.000)	6.4295 (1.000)	1.0044 (1.000)
DDPG-NF	3.6975 (0.548)	0.3767 (0.361)	2.5396 (0.395)	**0.3544 (0.353)**
Fuzzy 12345	4.4304 (0.657)	0.5694 (0.546)	3.5992 (0.560)	0.5453 (0.543)
Fuzzy 13555	4.3125 (0.639)	0.5186 (0.498)	3.3597 (0.523)	0.4961 (0.494)
Fuzzy 15555	4.3230 (0.641)	0.5001 (0.480)	3.3329 (0.518)	0.4778 (0.476)

(ii) Imperial Valley earthquake (1979), station: El Centro array #8, peak acceleration: 4.5696 m/s^2 (0.466 g), PEER database (near-fault)
(iii) Chi-Chi earthquake (1999), Station: TCU115, peak acceleration: 1.1531 m/s^2 (0.118 g), PEER database (far-field)
(iv) Loma Prieta earthquake (1989), station: agnews state hospital, peak acceleration: 1.580 m/s^2 (0.161 g), PEER database (far-field).

4.1 Control performance of the PSIS under the near-fault earthquakes

4.1.1 Near-fault El Mayor-Cucapah earthquake

The control performance of the PSIS system, designed based on the DRL control modules, was verified under the disturbance of the El Mayor-Cucapah earthquake for DDPG-NF, passive, fuzzy12345, fuzzy13555, and fuzzy15555 controllers, as illustrated in Fig. 11. Owing to space limitations, comparisons for the fuzzy12345 controller is provided only in figures, while the results for the passive, fuzzy13555 and fuzzy15555 controllers are presented in Table 2. This comparison assesses the superstructure acceleration, isolation layer displacement, clamping force of the PFD, and hysteresis loop for different controllers. The absolute maximum acceleration of the superstructure under various controllers are 6.747, 3.697, 4.430, 4.312, and 4.323 m/s^2 for passive, DDPG-NF, fuzzy 12345, fuzzy13555, and fuzzy 15555 controllers, respectively. Similarly, the absolute displacement of the isolation layer was recorded as 1.004, 0.354, 0.545, 0.496, and 0.477 m for respective controllers. The figures illustrate that the DDPG-NF control module outperforms all other controllers. Typically, in near-fault earthquakes, the primary control objective is to reduce response of the isolation layer displacement. Nevertheless, the DDPG-NF control module effectively suppresses both the isolation layer displacement and the superstructure acceleration responses, a challenging task in seismic control.

Generally, displacement response is mitigated by increasing system damping, stiffness, and control force, but acceleration response is often difficult to reduce and can even be amplified. Table 2 shows that the displacement response of the isolation layer during passive controller reaches 1.042 m, significantly exceeding the PSIS stroke limit of 0.15 m, highlighting the severity of the near-fault earthquake. The three fuzzy controllers for comparison exhibit a smaller range of control force than the DDPG-NF control module. Additionally, the isolation layer hysteresis loop for the DDPG-NF control module, shown in subplot (d) of Fig. 11, has the smallest area among the five controllers. This indicates that the DDPG-NF control module improves an energy dissipation capacity of the isolation system by increasing the friction of the PFD damper while reducing the isolation layer displacement. These detailed comparisons highlight the varied performance of each control strategy in managing the seismic response.

In summary, the isolation layer displacement to the DDPG-NF control was approximately 35% of that under passive control, and 74% of that under the second-best fuzzy15555 controller. The DDPG-NF controller demonstrates significantly superior performance, particularly under high intense near-fault earthquakes. This enhanced performance can be attributed to the higher demand for control force. Therefore, it is speculated that the difference in control performance would become even more pronounced with greater earthquake intensity. This indicates that the DDPG-NF control module improves an energy dissipation capacity of the isolation system by increasing the friction of the PFD damper while reducing the isolation layer displacement. These detailed comparisons highlight the varied performance of each control strategy in managing the seismic response.

Table 3 Response comparison of various controllers for near-fault EI Mayor-Cucapah earthquake

Control system	Superstructure		Isolation layer	
	Acceleration (m/s^2)	Displacement (m)	Acceleration (m/s^2)	Displacement (m)
Passive	1.9473 (1.000)	0.2647 (1.000)	1.6891 (1.000)	0.2530 (1.000)
DDPG-NF	2.4713 (1.269)	0.1324 (0.500)	1.2380 (0.733)	**0.1216 (0.481)**
Fuzzy 12345	1.7109 (0.879)	0.1991 (0.752)	1.3734 (0.813)	0.1901 (0.751)
Fuzzy 13555	2.1148 (1.086)	0.1746 (0.660)	1.2609 (0.746)	0.1654 (0.654)
Fuzzy 15555	2.2651 (1.163)	0.1486 (0.561)	1.1937 (0.708)	0.1392 (0.550)

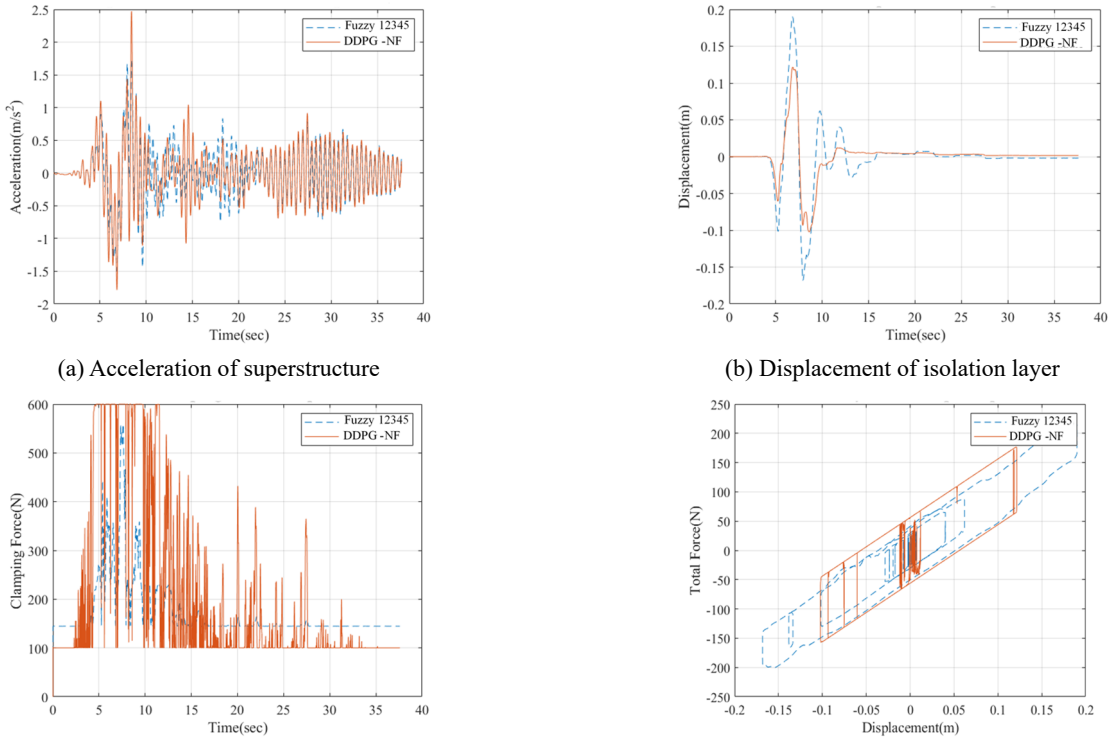

(a) Acceleration of superstructure

(b) Displacement of isolation layer

(c) PFD clamping force

(d) Hysteresis loop

Fig. 12 Response comparison between fuzzy12345, DDPG-NF controller under near-fault Imperial Valley earthquake

4.1.2 Near-fault Imperial Valley earthquake

Under the disturbance of the Imperial Valley earthquake, the control effectiveness of the DDPG-NF control module compared with other controllers is presented in Fig. 12. The absolute maximum response values are illustrated in Table 3 for the near-fault Imperial Valley earthquake. Similarly, due to space constraints, co mparison for the fuzzy12345 controller is exclusively provided in figures. In contrast, the results for the passive, fuzzy13555 and fuzzy15555 controllers are presented in Table 3. This approach ensures a clear and organized presentation of the different control performance within this study.

The results indicate that the absolute maximum acceleration of the superstructure under various controllers was 1.947, 2.471, 1.710, 2.114, and 2.265 m/s^2 for passive, DDPG-NF, fuzzy 12345, fuzzy 13555, and fuzzy 15555 controllers, respectively. Similarly, the absolute displacement of the isolation layer was recorded as 0.253, 0.121, 0.190, 0.165, and 0.139 m for the respective controllers. The DDPG-NF control module consistently exhibits the best performance in controlling the isolation layer displacement. However, it also results in less performance for superstructure acceleration among all the controllers, with an increase of about 27% compared to passive control. Alternatively, the displacement of the isolation layer is approximately 52% of that observed with passive control and 87% of the second-best fuzzy15555 control, maintaining the stroke limit of the PSIS. According to these results in Table 3, the DDPG-NF control module remains the most effective in suppressing isolation layer displacement, despite slightly amplifying the superstructure acceleration response, which is considered an acceptable trade-off.

Furthermore, the hysteresis loop in subplot (d) of Fig. 12 shows that the DDPG-NF control module appears to be wider and more rectangular compared to fuzzy12345. This indicates that the DDPG-NF module introduces more energy dissipation and control force during seismic events, which is beneficial for reducing structural responses. However, the DDPG-NF module demonstrates higher total forces (both positive and negative) across the same displacement range compared to the fuzzy12345 control. This suggests that the DDPG-NF module exerts more control force to maintain stability and reduce displacement during the near-fault earthquakes. The larger area enclosed by the DDPG-NF module loop indicates that it dissipates more energy compared to other controllers, thereby reducing the energy transmitted to the superstructure and enhancing seismic resilience. The comparison clearly shows that the DDPG-NF module provides a more robust control mechanism by applying higher forces and dissipating more energy, which are crucial for protecting the structure during near-fault seismic events. The fuzzy12345 controller, although effective, does not match the DDPG-NF control module performance, particularly in high-intensity scenarios.

According to the simulation results, two near-fault seismic dataset of varying intensities are tested to contrast the control efficacy of the DDPG-NF module with the respective controllers. The DDPG-NF control module demonstrated superior results in suppressing the displacement response of the isolation layer, outperforming other controllers in each near-fault earthquake test. The fuzzy15555 controller, designed with reference to the NSF

control system, ranked second in terms of control performance verification. Furthermore, it was observed that with low seismic intensity, the near-fault control module tends to amplify the superstructure acceleration response.

The DRL control module, trained using the DDPG algorithm, demonstrates exceptional effectiveness in managing near-fault earthquakes, as evidenced by detailed numerical simulations. The DDPG-NF control module consistently outperforms other control strategies, including passive control and various fuzzy controllers, in reducing the displacement of the isolation layer. This is crucial for maintaining structural integrity during high-intensity seismic events. For the El Mayor-Cucapah earthquake, the DDPG-NF control module significantly reduced the isolation layer displacement to approximately 35% of that under passive control and 74% of the second-best fuzzy controller, fuzzy15555. Additionally, the hysteresis loop analysis further indicates that the DDPG-NF module enhances the energy dissipation capacity of the isolation system, reducing the energy transmitted to the superstructure and thereby improving seismic resilience. Furthermore, in the case of Imperial Valley earthquake, the DDPG-NF module continued to demonstrate its superiority in controlling isolation layer displacement, achieving a 50% reduction compared to passive control. Although the superstructure acceleration was slightly higher compared to passive control, this trade-off is deemed acceptable due to the significant improvement in displacement control.

The DDPG-NF module ability to dissipate more energy, as evidenced by its wider and more rectangular hysteresis loop, further underscores its robustness in managing near-fault seismic events. As per the aforementioned results, the DRL control module trained by the DDPG algorithm is highly effective in enhancing the seismic resilience of structures during near-fault earthquakes. Its superior performance in reducing isolation layer displacement, coupled with its robust energy dissipation capabilities, makes it a powerful tool for protecting structures against high-intensity seismic events.

4.2 Control performance of the PSIS under the far-field earthquakes

4.2.1 Far-field Chi-Chi earthquake

The PSIS system control performance, designed using the DRL algorithm, was tested under two far-field earthquakes in addition to near-fault earthquake scenarios. The results, which include the superstructure acceleration, isolation layer displacement, PFD clamping force, and hysteresis loop response indices, are compared against passive control, a Deep Deterministic Policy Gradient model designed for Far-Field (DDPG-FF) control, and various sophisticated fuzzy control strategies (fuzzy12345, fuzzy13555, and fuzzy15555), as illustrated in Fig. 13.

Owing to space constraints, the results for fuzzy12345 are presented in the figures, while the results for passive, fuzzy13555 and fuzzy15555 are illustrated in Table 4. The absolute maximum acceleration of the superstructure recorded under different controllers was 2.690, 1.139, 1.851, 1.381, and 1.117 m/s^2 for passive, DDPG-FF, fuzzy12345, fuzzy13555, and fuzzy15555 controllers, respectively. Similarly, the absolute displacement of the isolation layer was 0.411, 0.112, 0.175, 0.137, and 0.120 m for the respective controllers.

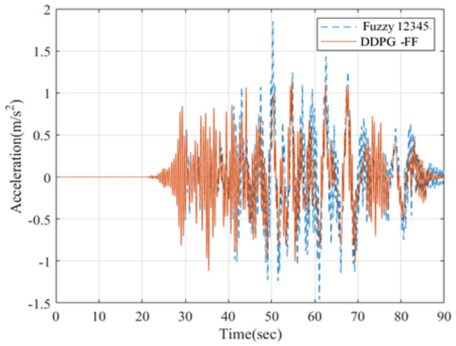

(a) Acceleration of superstructure

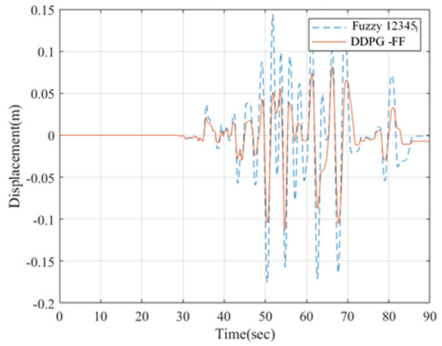

(b) Displacement of isolation layer

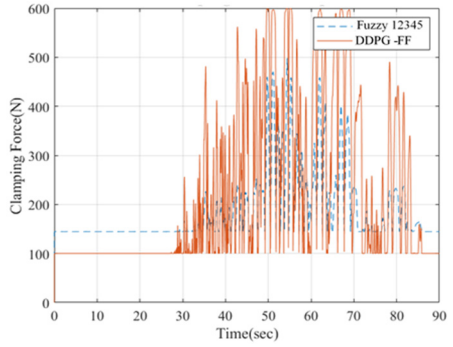

(c) PFD clamping force

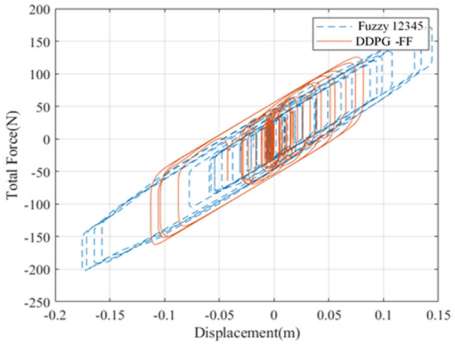

(d) Hysteresis loop

Fig. 13 Response comparison between fuzzy12345 and DDPG-FF controller under far-field Chi-Chi earthquake

Table 4 Response comparison of various controllers for the far-field Chi-Chi earthquake

Control system	Superstructure		Isolation layer	
	Acceleration (m/s^2)	Displacement (m)	Acceleration (m/s^2)	Displacement (m)
Passive	2.6908 (1.000)	0.4275 (1.000)	2.7046 (1.000)	0.4112 (1.000)
DDPG-NF	**1.1393 (0.423)**	0.1194 (0.279)	1.0542 (0.390)	0.1126 (0.274)
Fuzzy 12345	1.8519 (0.688)	0.1817 (0.425)	1.2984 (0.480)	0.1753 (0.426)
Fuzzy 13555	1.3812 (0.513)	0.1434 (0.335)	1.0853 (0.401)	0.1375 (0.334)
Fuzzy 15555	1.1173 (0.415)	0.1273 (0.298)	1.0777 (0.398)	0.1206 (0.293)

According to the subplot (c) of the Fig. 13 that the DDPG-FF control module demonstrates higher total force (both positive and negative) across the same displacement range compared to the fuzzy12345 controller. This suggests that the DDPG-FF module exerts higher control force, which is crucial for reducing displacements during the far-field earthquakes. At lower displacements, a more consistent force application is demonstrated by the DDPG-FF module, evident from the data points clustering tightly around the origin. This indicates effective control of small oscillations and maintaining structural integrity during minor seismic excitations. For larger displacements, this module shows a more significant force response, suggesting better handling of large seismic forces and providing greater resistance and stability during intense earthquakes. The comparison of hysteresis loops and clamping force reveals that the DDPG-FF control module demonstrates superior performance in terms of energy dissipation and force application compared to fuzzy12345 controller. This leads to improved seismic resilience, particularly during high-intensity seismic events, by attenuating displacement and enhancing the stability of the seismic isolation layer.

Furthermore, the subplot (d) of Fig. 13 shows that in an active time period (approximately between 30 to 70 seconds), the DDPG-FF control module shows a substantial increase in clamping force, adapting dynamically to the seismic activity. This suggests that the DDPG-FF module actively responds to changes in seismic intensity, applying higher forces when needed to maintain structural stability. On the other hand, the fuzzy12345 control remains relatively constant even during the active seismic period, which may not provide the same level of adaptability and response to high-intensity seismic events as the DDPG-FF module. Its constant clamping force may be adequate for moderate seismic conditions but might fall short during more intense events.

During the far-field Chi-Chi earthquake, the DDPG-FF module exhibited outstanding control performance, particularly in absolute maximum responses. The only exception was superstructure acceleration, where fuzzy15555 controllers outperformed slightly better. Notably, under passive controller, the maximum displacement response of the isolation layer reaches 0.4112 m, surpassing the PSIS stroke limit of 0.15 m, posing a threat even in non-near-fault earthquakes. Therefore, the DRL model prioritizes controlling isolation layer displacement, assigning it a higher weighting in its reward function. The results demonstrate that the DDPG-FF control module achieved approximately 27% reduction in isolation layer displacement compared to passive control, outperforming all other controllers. For maximum superstructure acceleration, the DDPG-FF control module achieved approximately 42% reduction compared to passive control, slightly inferior to the fuzzy15555 controller. Overall, the DDPG-FF control module showed commendable performance during the far-field Chi-Chi earthquake, indicating that the reward function design effectively guides the agent in determining suitable control parameters.

4.2.2 Far-field Loma Prieta earthquake

The effectiveness of the PSIS system, designed using the DRL algorithm, was also tested under far-field Loma Prieta earthquakes with medium PGA values. The results, which include the superstructure acceleration, isolation layer displacement, PFD clamping force, and hysteresis loop response indices as discussed in previous sections, are compared against passive control, DDPG-FF control, and various sophisticated fuzzy control strategies (fuzzy12345, fuzzy13555, and fuzzy15555) as illustrated in Fig. 14. Similarly, due to space constraints, comparison for the fuzzy12345 controller is exclusively provided in figures. In contrast, the results for the passive, fuzzy13555 and fuzzy15555 controllers are presented in Table 5. This approach ensures a clear and organized presentation of the different control performance within this study. The absolute maximum acceleration of the superstructure recorded for different controllers was 2.256, 1.245, 1.493, 1.166, and 1.203 m/s^2 for passive, DDPG-FF, fuzzy 12345, fuzzy 13555, and fuzzy 15555 controllers, respectively. Similarly, the absolute displacement of the isolation layer was 0.285, 0.040, 0.138, 0.091, and 0.051 m for the respective controllers.

Furthermore, the subplot (d) of Fig. 14 illustrates that the DDPG-FF control module exhibits a wider and more defined hysteresis loop, reaching higher total forces compared to the and fuzzy controls, indicating superior energy dissipation. Furthermore, both the passive and fuzzy controllers exhibit less consistent and effective control in comparison to the dynamic and higher energy dissipation capabilities of the DDPG-FF module, especially during high-intensity earthquake events. According to the Table 5, the isolation layer displacement response for the passive control was 0.2857 m, exceeding the PSIS stroke limit of 0.15 m, although it was slightly less than during the far-field Chi-Chi earthquake. Overall, the DDPG-FF control module demonstrated superior performance in suppressing the superstructure acceleration and isolation layer

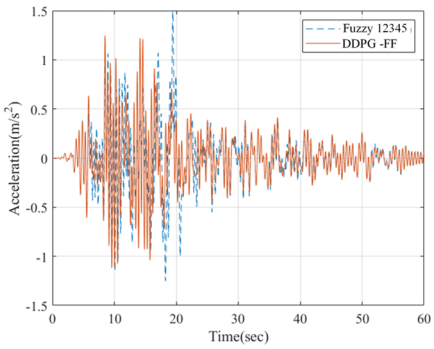

(a) Acceleration of superstructure

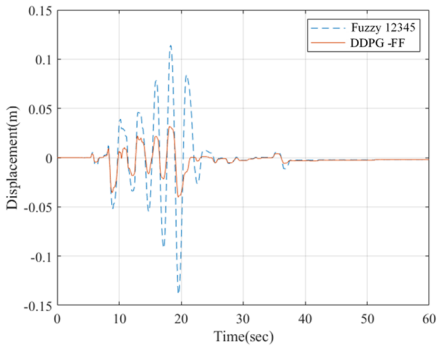

(b) Displacement of isolation layer

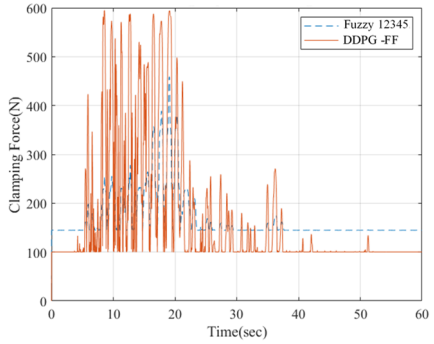

(c) PFD clamping force

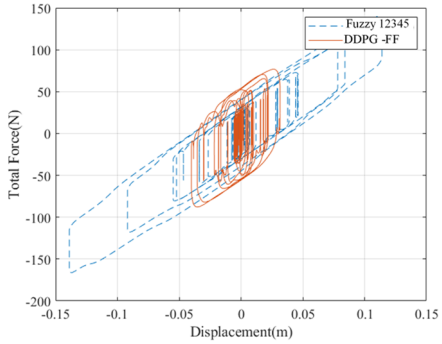

(d) Hysteresis loop

Fig. 14 Response comparison between fuzzy12345, DDPG-FF controller under far-field Loma Prieta earthquake

Table 5 Response comparison of various controllers for the far-field Loma Prieta earthquake

Control system	Superstructure		Isolation layer	
	Acceleration (m/s^2)	Displacement (m)	Acceleration (m/s^2)	Displacement (m)
Passive	2.2562 (1.000)	0.2965 (1.000)	1.9378 (1.000)	0.2857 (1.000)
DDPG-NF	**1.2452 (0.552)**	0.0427 (0.144)	0.6102 (0.315)	0.0401 (0.140)
Fuzzy 12345	1.4932 (0.662)	0.1447 (0.488)	1.0406 (0.537)	0.1389 (0.486)
Fuzzy 13555	1.1668 (0.517)	0.0942 (0.318)	0.7966 (0.411)	0.0911 (0.319)
Fuzzy 15555	1.2038 (0.534)	0.0542 (0.183)	0.6083 (0.314)	0.0518 (0.181)

displacement during this earthquake.

The DRL control module, trained with the DDPG algorithm, exhibited strong effectiveness and performance across various far-field earthquake scenarios in this study. Specifically designed for far-field earthquakes, the DRL module consistently surpassed passive control and other fuzzy control strategies in reducing the superstructure acceleration. During the Chi-Chi earthquake, the DDPG-FF module achieved notable reductions in both isolation layer displacement and superstructure acceleration decreasing by approximately 27% and the latter by about 42% compared to passive control. Although the fuzzy15555 controller slightly outperformed the DDPG-FF module in terms of superstructure acceleration, the DDPG-FF module still delivered commendable overall performance by effectively balancing displacement and acceleration. Additionally, during the Loma Prieta earthquake, the DDPG-FF module continued to demonstrate its strength, reducing isolation layer displacement by 14% and superstructure acceleration by 55% compared to passive control, through it was slightly less effective than the fuzzy15555 controller in this regard.

Throughout all two far-field earthquakes, the DRL control module consistently excelled in suppressing superstructure acceleration, outperforming both passive control and other fuzzy controllers. Its dynamic adaptability to different seismic intensities and its ability to effectively manage both displacement and acceleration effectively underscore the strength of the DDPG-trained DRL control module. Although the fuzzy controllers performed well in certain scenarios, particularly in controlling superstructure acceleration, the overall performance of the DDPG-FF module was superior.

5. Conclusions

This study presents a novel approach to enhancing the performance of an intelligent isolation system by employing a DDPG algorithm within a deep reinforcement learning framework. The proposed semi-active control strategy

addresses the shortcomings of traditional passive control techniques by dynamically adapting to diverse seismic intensities and characteristics, optimizing control parameters for effective performance under both near-fault and far-field earthquake conditions.

Numerical simulations validate the effectiveness of the DDPG-based control modules, showing significant improvements in attenuating isolation layer displacement and superstructure acceleration. Especially, the DDPG-NF module effectively mitigates displacement response of the isolation layer during near-fault earthquakes compared to other controllers. Conversely, the DDPG-FF control module excels in minimizing superstructure acceleration in far-field conditions, while remaining within the stroke limit of PSIS. Notably, DDPG-based control module achieves a substantial reduction in numerical simulation responses, decreasing the isolation layer displacement by approximately 52% in near-fault Imperial Valley earthquakes and reducing the acceleration of superstructure by approximately 57.65% during far-field Chi-Chi earthquakes.

The DDPG-trained DRL control module significantly enhanced energy dissipation, crucial for maintaining structural integrity in high-intensity seismic events. Its dynamic adaptability and robust performance across varying seismic intensities make it superior to traditional passive and fuzzy control strategies. This study highlights the enhancement of seismic resilience through the integration of advanced control techniques with semi-active systems. The adaptability of control parameters based on specific seismic conditions ensures optimal performance across a wide range of earthquake characteristics.

Acknowledgments

This research has been supported by the National Science and Technology Council under project number 113-2811-M-006-013.

References

Ali, T., Lee, J. and Kim, R.E. (2022), "Machine learning tool to assess the earthquake structural safety of systems designed for wind: In application of noise barriers", *Earthq. Struct.*, *Int. J.*, **23**(3), 315-328. https://doi.org/10.12989/eas.2022.23.3.315

Baker, J.W. (2007), "Quantitative classification of near-fault ground motions using wavelet analysis", *Bull. Seismol. Soc. Am.*, **97**(5), 1486-1501. https://doi.org/10.1785/0120060255

Bang, H., Yu, B. and Jeon, H. (2023), "Assembly performance evaluation method for prefabricated steel structures using deep learning and k-nearest neighbors", *Smart Struct. Syst.*, *Int. J.*, **32**(2), 111-121. https://doi.org/10.12989/sss.2023.32.2.111

Berhich, A., Belouadha, F.Z. and Kabbaj, M.I. (2023), "An attention-based LSTM network for large earthquake prediction", *Soil Dyn. Earthq. Eng.*, **165**, p. 107663. https://doi.org/10.1016/j.soildyn.2022.107663

Browne, C.B., Powley, E., Whitehouse, D., Lucas, S.M., Cowling, P.I., Rohlfshagen, P., Tavener, S., Perez, D., Samothrakis, S. and Colton, S. (2012), "A survey of Monte Carlo tree search methods", *IEEE Transactions on Computational Intelligence and AI in Games*, **4**(1), 1-43. https://doi.org/10.1109/TCIAIG.2012.2186810C

Degris, T., Pilarski, P.M. and Sutton, R.S. (2012), "Model-free reinforcement learning with continuous action in practice", In: *American Control Conference Fairmont Queen Elizabeth*, Montréal, Canada, pp. 2177-2182.

Deng, M., Sun, D., Zhan, L., Xu, X. and Zou, J. (2024), "Advancing active suspension control with td3-psc: integrating physical safety constraints into deep reinforcement learning", *IEEE Access*, **12**, 115628-115641. https://doi.org/10.1109/ACCESS.2024.3445663

Dolce, M., Cardone, D. and Marnetto, R. (2000), "Implementation and testing of passive control devices based on shape memory alloys", *Earthq. Eng. Struct. Dyn.*, **29**(7), 945-968. https://doi.org/10.1002/1096-9845(200007)29:7<945::AID-EQE958>3.0.CO;2

Eshkevari, S.S., Eshkevari, S.S., Sen, D. and Pakzad, S.N. (2023), "Active structural control framework using policy-gradient reinforcement learning", *Eng. Struct.*, **274**(2023), p. 115122. https://doi.org/10.1016/j.engstruct.2022.115122

Eswar, M., Chourasia, A. and Gopalakrishnan, N. (2022), "Seismic response control of buildings using shape memory alloys as smart material: State-of-the-Art review", *Earthq. Struct.*, *Int. J.*, **23**(2), 207-219. https://doi.org/10.12989/eas.2022.23.2.207

Fairbank, M. and Alonso, E. (2012), "The Divergence of Reinforcement Learning Algorithms with Value-Iteration and Function Approximation", In: *WCCI 2012 IEEE World Congress on Computational Intelligence*, June.

Fang, Y., Tee, K.F. and Yan, Y. (2024), "Computing of output of piezoelectric actuator under voltage excitation", *Smart Struct. Syst.*, *Int. J.*, **33**(5), 359-364. https://doi.org/10.12989/sss.2024.33.5.359

Florez, A.J., Giraldo, L.F. and Soto, M.G. (2024), "Regularized model-free adaptive control of smart base-isolated buildings", *Smart Struct. Syst.*, *Int. J.*, **34**(2), 73-85. https://doi.org/10.12989/sss.2024.34.2.073

Furnkranz, J., Hüllermeier, E., Cheng, W. and Park, S.H. (2012), "Preference-based reinforcement learning: A formal framework and a policy iteration algorithm", *Machine Learning*, **89**(2), 123-156. https://doi.org/10.1007/s10994-012-5313-8

Gzal, M., Carrion, J. E., AL-Shudeifat, M.A., Spencer, B.F., Conte, J.P., Vakakis, A.F., Bergman, L.A. and Gendelman, O.V. (2023), "Seismic mitigation of a benchmark twenty-story steel structure based on intermodal targeted energy transfer (IMTET)", *Eng. Struct.*, **283**, 1-13. https://doi.org/10.1016/j.engstruct.2023.115868

Hsu, T.Y., Huang, S.K., Chang, Y.W., Kuo, C.H., Lin, C.M., Chang, T Hsu, T.Y., Huang, S.K., Chang, Y.W., Kuo, C.H., Lin, C.M., Chang, T.M., Wen, K.L. and Loh, C.H. (2013), "Rapid on-site peak ground acceleration estimation based on support vector regression and P-wave features in Taiwan", *Soil Dyn. Earthq. Eng.*, **49**, 210-217. https://doi.org/10.1016/j.soildyn.2013.03.001

Kim, H.S., Roschke, P.N., Lin, P.Y. and Loh, C.H. (2006), "Neuro-fuzzy model of hybrid semi-active base isolation system with FPS bearings and an MR damper", *Eng. Struct.*, **28**(7), 947-958. https://doi.org/10.1016/j.engstruct.2005.09.029

Lee, S., Lee, J., Kim, M., Lee, S. and Lee, Y.J. (2024), "Deep learning-based anomaly detection in acceleration data of long-span cable-stayed bridges", *Smart Struct. Syst.*, *Int. J.*, **33**(2), 93-103. https://doi.org/10.12989/sss.2024.33.2.093

Lin, T.K., Lu, L.Y., Chuang, C.K. and Lin, T.K. (2023), "Development and Experimental Verification of an Intelligent Isolation System Based on Long Short-Term Memory Module Model for Ground Motion Characteristics Prediction", *Struct. Control Health Monitor.*, 2023, 1-25. https://doi.org/10.1155/2023/9770996

Liu, Y., Matsuhisa, H. and Utsuno, H. (2008), "Semi-active

vibration isolation system with variable stiffness and damping control", *J. Sound Vib.*, **313**(1-2), 16-28. https://doi.org/10.1016/j.jsv.2007.11.045

Lu, L.Y., Lin, C.C., Lin, G.L. and Lin, C.Y. (2010), "Experiment and analysis of a fuzzy-controlled piezoelectric seismic isolation system", *J. Sound Vib.*, **329**(11), 1992-2014. https://doi.org/10.1016/j.jsv.2009.12.025

Lu, L.Y., Lin, G.L. and Lin, C.Y. (2011), "Experiment of an ABS-type control strategy for semi-active friction isolation systems", *Smart Struct. Syst., Int. J.*, **8**(5), 501-524. https://doi.org/10.12989/sss.2011.8.5.501

Mnih, V., Kavukcuoglu, K., Silver, D., Rusu, A.A., Veness, J., Bellemare, M.G., Graves, A., Riedmiller, M., Fidjeland, A.K., Ostrovski, G., Petersen, S., Beattie, C., Sadik, A., Antonoglou, I., King, H., Kumaran, D., Wierstra, D., Legg, S. and Hassabis, D. (2015), "Human-level control through deep reinforcement learning", *Nature*, **518**(7540), 529-533. https://doi.org/10.1038/nature14236

Moerland, T.M., Broekens, J., Plaat, A. and Jonker, C.M. (2023), "Model-based reinforcement learning: A survey", *Foundations and Trends in Machine Learning*, **16**(1), 1-118. https://doi.org/10.1561/2200000086

Moustafa, A. and Takewaki, I. (2010), "Characterization and modeling of near-fault pulse-like strong ground motion via damage-based critical excitation method", *Struct. Eng. Mech., Int. J.*, **34**(6), 755-778. https://doi.org/10.12989/sem.2010.34.6.755

Mualla, I.H. and Belev, B. (2002), "Performance of steel frames with a new friction damper device under earthquake excitation", *Eng. Struct.*, **24**(3), 365-371. https://doi.org/10.1016/S0141-0296(01)00102-X

Naderpoor, P. and Taghikhany, T. (2022), "Seismic adaptive control of building structures with simultaneous sensor and damper faults based on dynamic neural network", *Comput.-Aided Civil Infrastr. Eng.*, **37**(11), 1402-1416. https://doi.org/10.1111/mice.12805

Noureldin, M., Ali, A., Nasab, M.S.E. and Kim, J. (2021), "Optimum distribution of seismic energy dissipation devices using neural network and fuzzy inference system", *Comput.-Aided Civil Infrastr. Eng.*, **36**(10), 1306-1321. https://doi.org/10.1111/mice.12673

Pavlidou, C. and Komodromos, P. (2020), "Peak seismic response of a symmetric base-isolated steel building: near vs. far fault excitations and varying incident angle", *Earthq. Struct., Int. J.*, **18**(3), 349-365. https://doi.org/10.12989/eas.2020.18.3.349

Pisarski, D. and Jankowski, L. (2023), "Reinforcement learning-based control to suppress the transient vibration of semi-active structures subjected to unknown harmonic excitation", *Comput.-Aided Civil Infrastr. Eng.*, **38**(12), 1605-1621. https://doi.org/10.1111/mice.12920

Shahi, S.K. and Baker, J.W. (2011), "An empirically calibrated framework for including the effects of near-fault directivity in probabilistic seismic hazard analysis", *Bull. Seismol. Soc. Am.*, **101**(2), 742-755. https://doi.org/10.1785/0120100090

Shi, D., Xu, Y., Demartino, C., Xiao, Y. and Spencer, B.F. (2024), "Cyclic behavior of laminated bio-based connections with slotted-in steel plates: Genetic algorithm, deterministic neural network-based model parameter identification, and uncertainty quantification", *Eng. Struct.*, **310**, 1-17. https://doi.org/10.1016/j.engstruct.2024.118114

Silver, D., Heess, N., Degris, T., Wierstra, D. and Riedmiller, M. (2014), "Deterministic policy gradient algorithms", *Proceedings of the 31st International Conference on Machine Learning*, **32**(1), 387-395.

Spudich, P., Rowshandel, B., Shahi, S.K., Baker, J.W. and Chiou, B.S.J. (2014), "Comparison of NGA-West2 directivity models", *Earthq. Spectra*, **30**(3), 1199-1221. https://doi.org/10.1193/080313EQS222M

Uhlenbeck, G.E. and Ornstein, L.S. (1930), "On the theory of the Brownian motion", *Phys. Rev.*, **36**, 823-841. https://doi.org/10.1103/PhysRev.36.823

Wang, B., Zhu, S. and Casciati, F. (2020), "Experimental study of novel self-centering seismic base isolators incorporating super-elastic shape memory alloys", *J. Struct. Eng.*, **146**(7), 1-16. https://doi.org/10.1061/(asce)st.1943-541x.0002679

Yang, J.N. and Agrawal, A.K. (2002), "Semi-active hybrid control systems for nonlinear buildings against near-field earthquakes", *Eng. Struct.*, **24**(3), 271-280. https://doi.org/10.1016/S0141-0296(01)00094-3

Zhao, Z., Chen, Q., Zhang, R., Jian, Y. and Pan, C. (2020), "A negative stiffness inerter system (NSIS) for earthquake protection purposes", *Smart Struct. Syst., Int. J.*, **26**(4), 481-493. https://doi.org/10.12989/sss.2020.26.4.481